Journal of Materials Science: Materials in Electronics (2019) 30:9897–9902
https://doi.org/10.1007/s10854-019-01327-8

(Al, Cu) Co-doped ZnS nanoparticles: structural, chemical, optical, and photocatalytic properties

B. Poornaprakash[1] · U. Chalapathi[1] · P. T. Poojitha[2] · S. V. Prabhakar Vattikuti[3] · M. Siva Pratap Reddy[4]

Received: 7 January 2019 / Accepted: 10 April 2019 / Published online: 12 April 2019

Abstract
The pristine and (Al, Cu) co-doped ZnS nanoparticles (NPs) were fabricated by a chemical refluxing approach at 100 °C for the first time. High resolution transmission electron microscopy images disclosed that the fabricated NPs were visually spheroid shaped. The X-ray diffraction and micro Raman spectroscopy results stipulated that (Al, Cu) co-doped ZnS NPs were effectively procured with zincblende structure without the existence of foreign phases. A reduction in the optical band gap was obtained in the ZnS NPs after (Al, Cu) co-doping. The photoluminescence (PL) of pristine ZnS was totally quenched through (Al, Cu) co-doping. Malachite green was degraded by using pristine and (Al, Cu) co-doped ZnS NPs under the simulated solar light illumination. Higher degradation efficiency was obtained through (Al, Cu) co-doped catalyst compared with the pristine ZnS catalyst. The (Al, Cu) co-doped ZnS NPs displayed the hydrogen production rate of 4994.7 m mol g^{-1} h^{-1} in 300 min under simulated solar light irradiation. Hence, (Al, Cu) co-doping is a novel and promising path to enrich the photocatalytic degradation and the hydrogen production of the pristine ZnS NPs.

1 Introduction

Currently, new methods for obtaining interesting electronic, optical, and photochemical properties of nanocrystals are enticing mighty attention as expectation for diverse applications [1, 2]. Among the various semiconductor compounds, ZnS is an allured candidate that has been investigated enormously as a significant phosphor for various applications, since it has large exciton binding energy, large band gap and chemical stability. Frequently, doped nanocrystals can extend the physical properties as well as the raises the optical absorption, which controls the band gap energies, shaped it fit for photocatalytic degradation and hydrogen production. The past few years, there have been several interesting reports available on the hydrogen production of different composites [3–7]. Recently, many researchers reported the high activity of hydrogen production in ZnS even without any assistance of noble metal co-catalyst [8, 9]. Due to its wide band gap, the theoretical efficiency of photocarrier generation of this compound is ample higher than that of titanium dioxide, which may be greatly beneficial to the photocatalytic activity. However, the efficiency of this compound is gravely cramped through the quick recombination of photoexcited charge carriers. In addition, due to its large and gap, which could restrict its ability for solar energy harvesting. Therefore, the photocatalytic activity of ZnS can still be immensely ameliorated. It is believed that, ZnS will be a favorable candidate for effective solar water splitting, when its direct recombination of charge carriers is repressed. Therefore, enormous efforts have been dedicated to either or reducing the recombination of photogenerated charge carriers or narrowing the band gap and of ZnS. According to the current research results, doped ZnS systems may become a feasible key to remarkably develop the photocatalytic hydrogen production activity of ZnS [10, 11]. The past few years, several interesting reports available on the enhanced photocatalytic activity of the doped ZnS systems [12–14]. Now, the focus turns to the co-doped ZnS catalysts. More recently, Gang et al. [15] reported the

✉ B. Poornaprakash
mail2poorna6@gmail.com

✉ M. Siva Pratap Reddy
dr.mspreddy@gmail.com

[1] Department of Electronic Engineering, Yeungnam University, Gyeongsan 38541, South Korea

[2] Department of Physics, Siddartha Educational Academy Group of Institutions, Tirupati 517502, India

[3] School of Mechanical Engineering, Yeungnam University, Gyeongsan 38541, South Korea

[4] School of Electronics Engineering, Kyungpook National University, Daegu 41566, South Korea

enhanced photocatalytic activity of (In and Cu) co-doped ZnS nanoparticles. Melody et al. [16] also noticed the effective H_2 production in the (Ga, Cu) co-doped ZnS nanoparticles through hydrothermal route. This has stimulated the present authors to investigate the photocatalytic activity of co-doped ZnS system.

In this study, pristine and (Al, Cu) co-doped ZnS NPs were fabricated via chemical refluxing approach. The structural, optical, luminescence, photocatalytic degradation and hydrogen evolution properties were analyzed and achieved the enhanced photocatalytic activity of the ZnS NPs through (Al, Cu) co-doping.

2 Synthesis and characterizations

Pristine and (Al, Cu) co-doped ZnS NPs were prepared through the chemical refluxing route at 100 °C. For pristine ZnS, 0.05 M of zinc acetate (0.548 g) was dissolved in 50 ml of the distilled water and magnetically stirred for 10 min at 50 °C. Next, 0.05 M of sodium sulfide (0.622 g) solution (50 ml) was added to the above zinc solution and the mixture (white) was refluxed for 5 h at 100 °C. After that, the obtained product was centrifuged and rinsed with ethanol. Finally, annealed at 100 °C for 12 h in an oven. For, (Al, Cu) co-doped ZnS, 0.05 M of zinc acetate (0.504 g), copper chloride (0.017 g) and aluminum chloride (0.024 g) were dissolved in 50 ml of the distilled water and magnetically stirred for 10 min at 50 °C. Next, 0.05 M of sodium sulfide (0.622 g) solution (50 ml) was added to the above solution and the mixture (dark green) was refluxed for 5 h at 100 °C. Next, the obtained product was centrifuged and rinsed with ethanol. Finally, annealed at 100 °C for 12 h in an oven.

The high resolution transmission electron microscope (HRTEM) images were recorded through Philips Tecnai FE 12 model. The X-ray diffraction (XRD) patterns of the prepared samples were recorded using PANalytical diffractometer with Cu-Kα radiation. Micro-Raman spectra were recorded using Nicolet 6700 model Raman spectrometer. The diffuse reflectance spectra (DRS) were recorded with a Carry-5000 UV–vis-NIR double-beam spectrophotometer. Photoluminescence spectra were carried out by JOBIN YVON Fluorolog-3 spectrometer with a 450 W Xenon arc lamp as an excitation source. X-ray photoelectron spectroscopy measurements were recorded with Thermo Scientific K-Alpha XPS, using an Al Kα X-ray source (1486.6 eV). The photocatalytic degradation of the Malachite green dye was accomplished under artificial solar light radiation using a MaX 303 Xe lamp of 300 W power and 50 mW/cm^2 light intensity. Prior to irradiation, a solution holding 100 mg of the sample as well as the 100 mL of the Malachite green solution was stirred for 30 min in the dark. At every 5 min interval, 5 mL of the reaction solution was taken and quickly centrifuged to find the influence of Malachite green adsorption on the catalyst. The obtained solutions were investigated using a UV–Vis spectrometer (Cary, 5000).

3 Results and discussions

3.1 HRTEM studies

Figure 3 illustrates the HRTEM images of (a) pristine ZnS and (b) (Al, Cu) co-doped ZnS NPs and revealed that the fabricated NPs are tiny polydispersed with virtually spherical shaped. No amendment in the spherical morphology was found in the pristine NPs after co-doping. The calculated average size of the fabricated samples was 5.2 and 4.6 nm for pristine and (Al, Cu) co-doped ZnS, respectively. The size of the (Al, Cu) co-doped ZnS NPs are smaller than their pristine ZnS counterparts proposed that the growth rate of the co-doped NPs was limited by the difference in the ionic radii of the Al and Cu dopant [17]. The inset of Fig. 1 shows the lattice fringes with 0.325 and 0.319 nm of pristine and (Al, Cu) co-doped ZnS NPs and as agreed well with that of d-spacing (111 plane) of bulk ZnS.

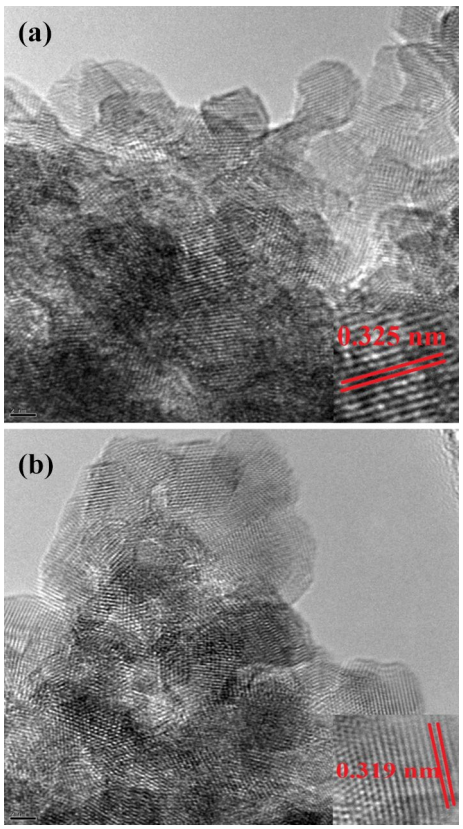

Fig. 1 HRTEM images of **a** pristine and **b** (Al, Cu) co-doped ZnS nanoparticles

3.2 XRD studies

The structure identification along with phase purity of both pristine and (Al, Cu) co-doped ZnS NPs were analyzed through XRD as depicted in Fig. 2 and display a cubic zinc-blende structure of bulk ZnS and agreed well with JCPDS card No: 50-0005. The widening of the diffraction peaks shows the nano regime of the fabricated samples. The effects of (Al, Cu) substitution into the ZnS nanoparticles are evident from the slight shift of the XRD peaks to a higher angle with (Al, Cu) co-doping. This shift indicates successful doping of Al and Cu ions in the ZnS host lattice. Furthermore, no foreign peaks found in both the fabricated samples, resulted in the impurity-free NPs. The average crystallite size of the as-fabricated samples, D_{hkl}, can be assessed through the Scherrer's formula [17]. The calculated crystallite sizes were 4.4 nm and 3.9 nm for pristine and (Al, Cu) co-doped ZnS NPs, respectively.

3.3 Raman studies

Figure 3 displays the micro- Raman spectra of the pristine and (Al, Cu) co-doped ZnS NPs. From these spectra, we noticed two Raman modes around 263 cm^{-1} and 351 cm^{-1}, which clearly matched well with the cubic phase ZnS (bulk) [18, 19]. A trivial shift of the Raman modes towards to lower frequency side recognized in pristine sample after (Al, Cu) co-doping, which is due to the strain caused through Al and Cu ions. This shift also indicates that the effective substitution of the Al and Cu ions in the ZnS lattice. No Raman modes associated with impurity phases were noticed in the samples, suggesting that the purity of the prepared NPs.

3.4 DRS and PL studies

Figure 4 shows the DRS spectra of pristine and (Al, Cu) co-doped ZnS NPs. The absorption edges of the (Al, Cu) co-doped sample red shifted than that of pristine ZnS, which also indicates the successful penetration Al and Cu ion in the

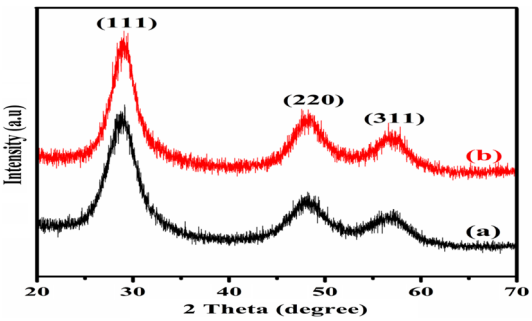

Fig. 2 XRD patterns of (a) pristine and (b) (Al, Cu) co-doped ZnS nanoparticles

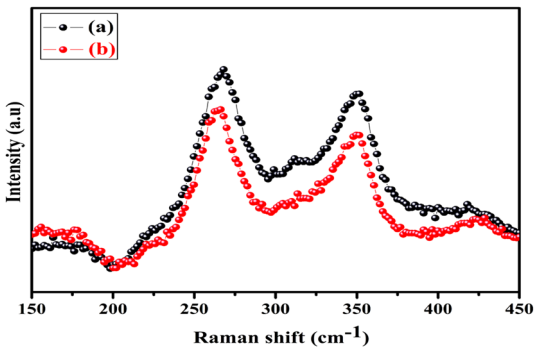

Fig. 3 Raman spectra of (a) pristine and (b) (Al, Cu) co-doped ZnS nanoparticles

host matrix and which may due to the *sp-d* exchange interaction among the dopants (Al and Cu) as well as the host (ZnS) and is the most frequent phenomena in transition metals doped II-VI semiconductor compounds [17]. The band gap energies of these NPs were assessed from DRS spectra by plotting the energy and extrapolating the linear part of the curve of $F(R)^2 = 0$ against the square of the Kubelka–Munk function F (R) as illustrated in Fig. 5. The obtained values are 3.41 eV and 3.30 eV for pristine and (Al, Cu) co-doped ZnS NPs, respectively.

The intrinsic as well as the extrinsic defects in wide band gap semiconductor compounds may be investigated through the nondestructive PL measurements and its provides information about the impurity and defect energy states even when they are present in very minute concentrations and therefore is useful to understand defect structures in semiconductor compounds. Figure 6 displays the PL spectra of the pristine and (Al, Cu) co-doped ZnS NPs with an excitation wavelength of 325 nm. The spectra comprise a wide emission band ranging from 350 to 550 nm. Although, the PL intensity of the pristine ZnS was decreased after (Al, Co) co-doping. The broad emission may be originating from

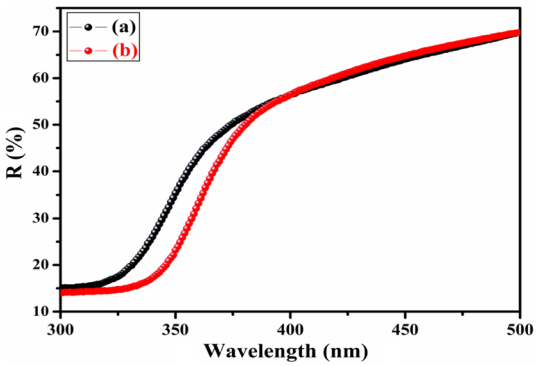

Fig. 4 DRS spectra of (a) pristine and (b) (Al, Cu) co-doped ZnS nanoparticles

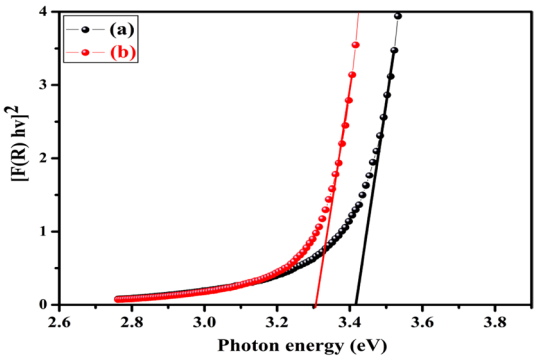

Fig. 5 Kubelk-Munk plots of (a) pristine and (b) (Al, Cu) co-doped ZnS nanoparticles

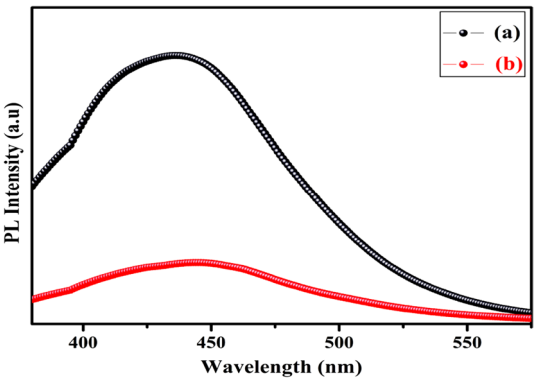

Fig. 6 PL spectra of (a) pristine and (b) (Al, Cu) co-doped ZnS nanoparticles

the surface defect states such as sulfur vacancies located at the surface of ZnS nanoparticles [20, 21]. Similar blue and broad emission was reported by several earlier workers [22–24] also and was due to surface defect states of the ZnS nanoparticles. Distinctly, this emission does not correspond to band edge luminescence of ZnS, since, the band gap lies in the range of 3.30–3.41 eV as may be seen from Fig. 5. The PL quenching of the (Al, Cu) co-doped NPs induced by the Al and Cu doping, proves the decrement of the recombination of electron–hole pairs. Similar emission quenching was reported by huge earlier researchers in doped and co-doped ZnS systems, however, no reports available on the PL property of (Al, Cu) co-doped ZnS to compare our results with them.

3.5 XPS studies

To explore the chemical composition along with chemical states of the elements present in the (Al, Cu) co-doped ZnS NPs, an XPS survey scan of (Al, Cu) co-doped ZnS NPs are displayed in Fig. 7. The peaks due to Zn are located at 1022.83 (Zn $2p_{3/2}$) and 1045.94 eV (Zn $2p_{1/2}$), respectively,

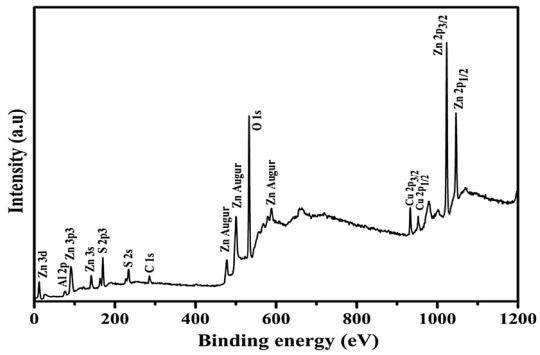

Fig. 7 XPS spectrum of (Al, Cu) co-doped ZnS nanoparticles

as depicted in Fig. 7 (a) and proposing that the chemical state of Zn is divalent (+2). The Al peak was located at 74.03 eV corresponds to the binding of the core level Al 2p, displaying that the oxidation state of the Al ions in the ZnS NPs is +3. The peaks related to Cu are located at 931.92 (Cu $2p_{3/2}$) and 951.90 eV ($Cu2p_{1/2}$), respectively, affirm the existence of Cu in the host matrix as +2. The peak of S is located at 161.69 eV and belongs to S 2p, indicating the −2 valence state of the S. The atomic percentages of the Zn, Al, Cu and S are found to be 48.01, 1.95, 2.06, and 47.98, respectively. Furthermore, no peaks belonging to the secondary phases of Al or Cu were found in the (Al, Cu) co-doped ZnS NPs.

3.6 Photocatalytic degradation and H_2 evolution studies

In the present work, we utilized both pristine and (Al, Cu) co-doped ZnS NPs as Sorbents for the Malachite green dye degradation in a solution under the simulated solar light illumination. A decrement in the band gap of the (Al, Cu) co-doped ZnS NPs was found, that's strive us to undertake the Malachite green dye degradation under simulated solar light illumination. Figure 8 illustrates the UV–Vis absorption spectra of Malachite green with irradiation time at the (a) pristine and (b) (Al, Cu) co-doped ZnS NPs. For 100% degradation of Malachite green in aqueous solution, 60 and 35 min were taken from pristine and (Al, Cu) co-doped ZnS NPs, respectively. A graph among C/C_0 and time indicates that the (Al, Cu) co-doped ZnS NPs was able to degrade Malachite green quicker than the pristine NPs, as shown in Fig. 9. Figure 10 displays the photocatalytic degradation kinetics of the Malachite green solution for the pristine and (Al, Cu) co-doped ZnS NPs under the simulated solar light illumination. Figure 11 shows the stability of the (Al, Cu) co-doped ZnS catalyst for the durative reaction process. We strongly believed that the enhanced photocatalytic activity of the (Al, Cu) co-doped ZnS NPs may be due to narrowing bandgap induced by the Al and Cu co-doping. In addition, the PL intensity of the (Al, Cu) co-doped ZnS diminishes

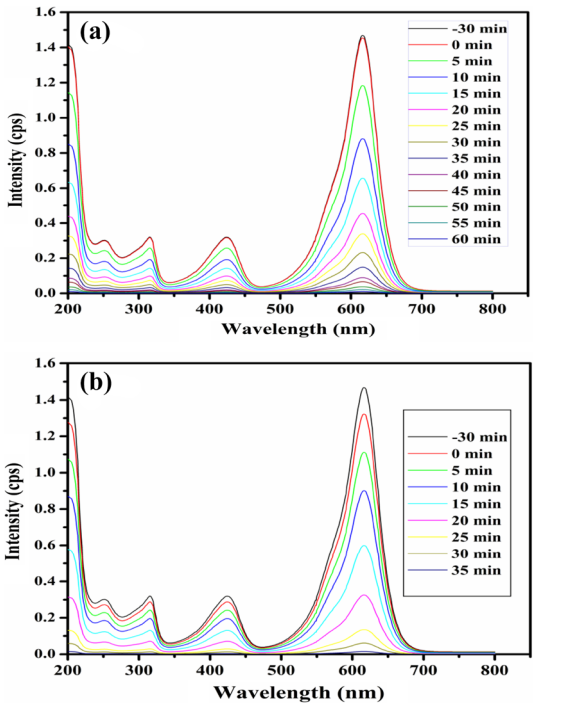

Fig. 8 UV–Vis absorption spectra changes of Malachite green aqueous solution in the presence of **a** pristine and **b** (Al, Cu) co-doped ZnS nanoparticles

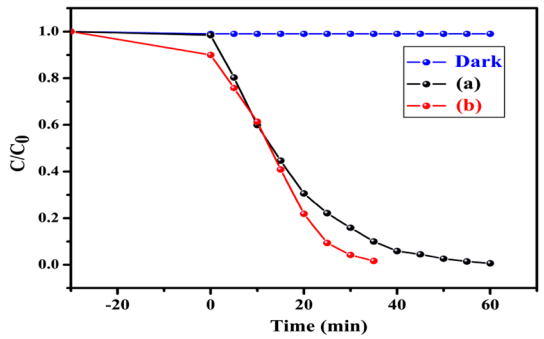

Fig. 9 Photocatalytic activities of (a) pristine and (b) (Al, Cu) co-doped ZnS nanoparticles

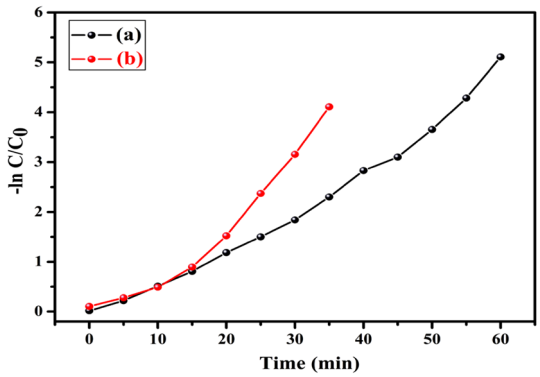

Fig. 10 Kinetic linear simulations of Malachite green photocatalytic degradation over the (a) pristine and (b) (Al, Cu) co-doped ZnS nanoparticles

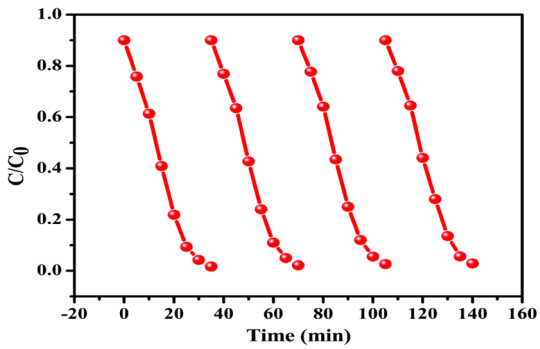

Fig. 11 Photocatalytic recycling test over the (Al, Cu) co-doped ZnS nanoparticles

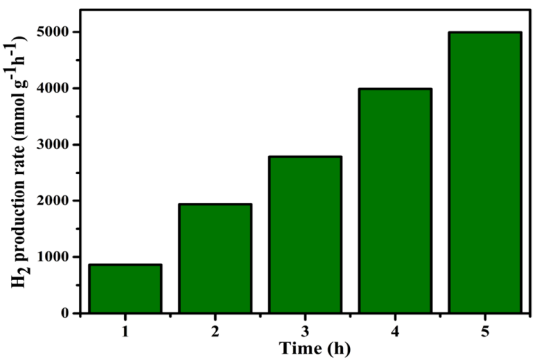

Fig. 12 Photocatalytic H2 production over the (Al, Cu) co-doped ZnS nanoparticles under the simulated solar light illumination

appreciably as the Al and Cu co-doping upon the visible light region of 350–550 nm. The PL quenching induced by the Al and Co co-doping, manifests the decrement of the recombination of electron–hole pairs.

Photocatalytic H_2 evaluation activities of (Al, Cu) co-doped ZnS NPs were assessed under 300 W Xenon lamp using mixed 0.2 M Na_2SO_3/0.3 M Na_2S aqueous solutions as scavengers. Figure 12 depicts the H_2 evolution from water splitting over (Al, Cu) co-doped ZnS NPs as catalyst and showed H_2 production of 4994.7 m mol g^{-1} h^{-1} in 300 min. It is well known that narrowing the bandgap and reducing the recombination of photogenerated charge carriers are the major hurdles for the enhanced photocatalytic activity. We can correlate the H_2 production of (Al, Cu) co-doped ZnS catalyst with DRS and PL data, we can propose a decreased band gap as well as the reduced recombination of electron–hole pairs are the causes for the present

H_2 production. Hence, the (Al, Cu) co-doped ZnS NPs are promising candidates for the H_2 production. Recently, Gang et al. [15] obtained the improved photocatalytic activity in indium and copper co-doped ZnS nanoparticles. Melody et al. [16] observed the effective H_2 production in the (Ga, Cu) co-doped ZnS nanoparticles.

4 Conclusions

In summary, pristine and (Al, Cu) co-doped ZnS NPs were fabricated via a chemical refluxing route at 100 °C. HRTEM images divulged the as-prepared NPs were slightly polydispersed with spheroid shaped. Both XRD and Raman results designated that effective entry of Al, Cu ions in the ZnS matrix without changing its zincblende phase. A redshift in the absorption edge was noticed in the ZnS after (Al, Cu) co-doping. The emission of pristine NPs was totally quenched through (Al, Cu) co-doping. XPS results indicated that the existence of Al and Cu in the host matrix as +3 and +2 states. Higher degradation (Malachite green dye) efficiency was obtained through (Al, Cu) co-doped catalyst compared with the pristine catalyst. In addition, (Al, Cu) co-doped catalyst achieved the maximum hydrogen production of 4994.7 m mol g^{-1} h^{-1} in 300 min under simulated solar light irradiation. Thus, (Al, Cu) co-doping is a novel approach to extend the photocatalytic degradation as well as the hydrogen production rate of the pristine ZnS NPs.

Acknowledgements This work was supported by the National Research Foundation of Korea (NRF) funded by Ministry of Education funded by the Ministry of Science, ICT and Fusion Research (2018R1D1A1B07040603) and BK21 Plus funded by the Ministry of Education (21A20131600011).

References

1. T. Dietl, H. Ohno, Rev. Mod. Phys. **86**, 187 (2014)
2. I.V. Martynenko, A.P. Litvin, F. Purcell-Milton, A.V. Baranov, A.V. Fedorov, Y.K. Gun'ko, J. Mater. Chem. B **5**, 6701 (2017)
3. A. Sobhani-Nasab, S. Pourmasoud, F. Ahmadi, M. Wysokowski, T. Jesionowski, Mater. Lett. **238**, 159 (2019)
4. H. Kooshki, A. Sobhani-Nasab, M. Eghbali-Arani, F. Ahmadi, V. Ameri, M. Rahimi-Nasrabadi, H. Ehrlich, M. Rahimi-Nasrabadi, Sep. Purif. Technol. **211**, 873 (2019)
5. F. Sedighi, M. Esmaeili-Zare, A. Sobhani-Nasab, M. Behpour, J. Mater. Sci. Mater. Electron. **29**(16), 13737 (2018)
6. M. Rahimi-Nasrabadi, M. Behpour, A. Sobhani-Nasab, S.M. Hosseinpour-Mashkani, J. Mater. Sci. Mater. Electron. **26**(12), 9776 (2015)
7. M. Rahimi-Nasrabadi, M. Behpour, A. Sobhani-Nasab, M.R. Jeddy, J. Mater. Sci. Mater. Electron. **27**(11), 11691 (2016)
8. J. Zhang, Yu. J, Y. Zhang, Q. Li, J.R. Gong, Nano Lett. **11**(11), 4774 (2011)
9. Y. Hong, J. Zhang, X. Wang, Y. Wang, Z. Lin, Y. Jiaguo, F. Huang, Nanoscale **4**, 2859 (2012)
10. J. Zhang, Y. Wang, J. Zhang, Z. Lin, F. Huang, Y. Jiaguo, ACS Appl. Mater. Interfaces **5**, 1031 (2013)
11. P. Weide, K. Schulz, S. Kaluza, M. Rohe, R. Beranek, M. Muhler, Langmuir **32**, 12641 (2016)
12. G.-J. Lee, S. Anandan, S.J. Masten, J.J. Wu, Renew. Energy **89**, 18 (2016)
13. B. Poornaprakash, U. Chalapathi, S.V.P. Vattikuti, M.C. Sekhar, B. Purusottam Reddy, P.T. Poojitha, M.S.P. Reddy, Y. Suh, S.H. Park, Ceram. Int. **45**, 2289 (2019)
14. B. Poornaprakash, U. Chalapathi, Y. Suh, S.P. Vattikuti, M.S.P. Reddy, S.H. Park, Ceram. Int. **44**, 11724 (2018)
15. G.-J. Lee, H.-C. Chen, J.J. Wu, Int. J. Hydrog. Energy **44**(1), 110 (2018)
16. M. Kimi, L. Yuliati, M. Shamsuddin, J. Nanomater. **16**(1), 195024 (2015)
17. B. Poornaprakash, U. Chalapathi, B. Purusottam Reddy, P.T. Poojitha, S.H. Park, J. Alloys Compd. **705**, 51 (2017)
18. B. Poornaprakash, P.T. Poojitha, U. Chalapathi, S. Ramu, R.P. Vijayalakshmi, S.H. Park, Ceram. Int. **42**, 8092 (2016)
19. B. Poornaprakash, S. Ramu, S.H. Park, R.P. Vijayalakshmi, B.K. Reddy, Mater. Lett. **164**, 104 (2016)
20. B. Poornaprakash, D. Amaranatha Reddy, G. Murali, N. Madhusudhana Rao, R.P. Vijayalakshmi, B.K. Reddy, J. Alloys Compd. **577**, 79 (2013)
21. B. Poornaprakash, S. Sambasivam, D. Amaranatha Reddy, G. Murali, R.P. Vijayalakshmi, B.K. Reddy, Ceram. Int. **40**, 2677 (2014)
22. N. Karar, F. Singh, B.R. Mehta, J. Appl. Phys. **95**, 656 (2004)
23. P.K. Ghosh, S.F. Ahmed, S. Jana, K.K. Chattopadhyay, Opt. Mater. **29**, 1584 (2007)
24. W.Q. Peng, G.W. Cong, S.C. Qu, Z.G. Wang, Opt. Mater. **29**, 313 (2006)